ELSEVIER

Fluid Phase Equilibria 158–160 (1999) 37–47

FLUID PHASE EQUILIBRIA

A comparison of molecular-based models to determine vapor–liquid phase coexistence in hydrogen fluoride

Donald P. Visco Jr., David A. Kofke *

Department of Chemical Engineering, State University of New York at Buffalo, Buffalo, NY 14260, USA

Received 22 March 1998; accepted 22 September 1998

Abstract

In this work, we apply the Gibbs–Duhem integration (GDI) technique to obtain the vapor–liquid equilibrium (VLE) properties of hydrogen fluoride according to three potential models. Properties examined include coexistence densities, enthalpy of vaporization, and vapor pressure. The models are representative of the various types of potentials used in simulation studies; namely, a pure pair potential from *ab initio* studies, an effective pair potential which fits parameters to condensed phase properties, and a semi-empirical pair potential. The effective pair potential was found to be the best performer of the three potentials tested, with semi-quantitative agreement with experiment. The other potentials which, by definition, did not include 3+ body effects performed poorly at most states. The effective pair potential is used to specify parameters in a Statistical Associating Fluid Theory (SAFT) model for hydrogen fluoride (HF). Significant improvement is seen over previous attempts to model HF using SAFT, although shortcomings do remain.

Keywords: Molecular simulation; Hydrogen fluoride; Association; Vapor–liquid equilibria; Vapor pressure; SAFT

1. Introduction

The open literature is filled with computer simulations of potential models which have been proposed to describe molecular interactions in real systems. Some models are studied only to provide qualitative insight, while others are meant to be useful for quantitative calculation. For the latter the quality of the model is judged on the extent to which a set of predicted thermodynamic quantities compares with experimental data; the closer the agreement, the better the model. At the industrial level, the next step is to utilize the accurate models to explore quickly and inexpensively the vast sets of temperature, pressure and composition of interest via simulation at all stages of process develop-

* Corresponding author. Tel.: +1-716-645-2911; fax: +1-716-645-3822; e-mail: kofke@eng.buffalo.edu

0378-3812/99/$ - see front matter
PII: S0378-3812(99)00132-6

ment. Predictive ability is important yet relative; a wide range of accuracies (say from 1% to 50%) may be judged adequate depending on the property being modeled and the stage of the process design for which the data are needed. Still, relatively few models have been formulated that can describe real compounds to a useful degree [1]. Part of the problem stems from the limited range of properties that have been considered in a model's development. A good outcome for the liquid density and energy does not guarantee a reasonable prediction of the vapor pressure (for example). Likewise, in materials for which good pure-fluid potential models exist, there is the added difficulty of determining cross-interactions when applied to the prediction of mixture properties.

For some systems, such as hydrogen fluoride (HF), the motivating factor in potential model development is not only expense but safety as well. HF is notoriously difficult to work with owing to its caustic and toxic nature. Thus, experimental data for this compound are scarce at many industrially important states. It is thought that one area where simulation of HF can be utilized is in providing data where no experiments have yet been performed.

An added role for detailed molecular models is in the formulation of coarse-grained molecular-based engineering models. The Statistical Associating Fluid Theory (SAFT) is such a model [2]. The parameters of this model are defined with reference to a coarse molecular picture, nevertheless these parameters are often specified by fitting to experiment. It would be desirable to find that they can instead be given by fitting to a molecular model that has been shown to yield properties that are close to experiment.

Parameters in intermolecular potential models which are used to describe real systems such as HF are based, in part or in full, on *ab initio* data and/or experimental data. The utility of both these data types and the incorporation of higher-than-pair interactions into the model is how we will distinguish the various potentials. A pure pair potential for HF is that which is based solely on *ab initio* data on the dimer. On the opposite end of the spectrum are the effective pair potentials which incorporate the effects of 3 + body interactions through fitting the model parameters to condensed phase experimental data. Somewhere in between, but closer to the former than latter, are semi-empirical pair potentials. This group does not incorporate higher-than-pair interactions into the model in any way, but does utilize experimental information on the dimer to adjust the parameters of the potential.

There has been a variety of potential models used to describe HF interactions in both the condensed and vapor phases. For the liquid potentials [3–11] where development is primarily for use in simulation studies and thus has a goal of providing bulk phase properties, the models tend to be more concise with limited distinctions between various types of attractions or repulsions. In the vapor [12–15], where concern has mainly been determination of various modal frequencies, models are more finely developed and employ (in some cases) parameters numbering an order of magnitude more than the liquid potentials. The greater than two-body interactions in the gas phase, which are negligible for many species, are profoundly important in HF vapor. However, the determination of bulk properties in the vapor via these potentials was not the goal of these researchers and so the incorporation of these terms at a level of theory on par with the pair interactions is limited [16].

It would be interesting to explore the ability of each of the three types of potentials to describe a useful property of HF, namely, the vapor–liquid coexistence curve. To this end, we have performed vapor–liquid equilibria (VLE) calculations on one pure pair potential, one effective pair potential and one semi-empirical pair potential.

The rest of the paper sets up as follows. Section 2 provides background on the potential models used and, in the simpler cases, the potential itself. Section 3 describes the computer simulation

techniques invoked to complete the VLE study. In Section 4 we present the coexistence densities as well as the heat of vaporization and vapor pressure. Section 5 contains a discussion of the results, and shows how one of the molecular models can be used to improve the performance of a SAFT-based model in describing HF properties. Section 6 offers concluding remarks.

2. Intermolecular potential models

2.1. W.L. Jorgensen (J79)

Jorgensen published two *ab initio* fitted potential models for HF; one in 1978 which used a double-zeta basis set [17] and a second in 1979 which used a minimal basis set [5]. The former fit employs a two-site model with coulombic interactions between the sites and r^{-3}, r^{-6} and r^{-12} interactions between the atom centers. The latter fit used the same model except that a third charge site was included. Additionally, the former fit was scaled to reproduce the experimental energy of vaporization so it is not a 'true' pair potential while the latter is a true pair potential [5]. Thus, the model published in 1979 is an example of the first type of potential model, namely, an *ab initio* derived model which uses only pair interactions. The intermolecular potential between two molecules from this model then written as

$$u_{i,j} = \sum_{Vi}\sum_{Wj}\left(q_{Vi}q_{Wj}/r_{Vi,Wj}\right) + \sum_{Si}\sum_{Tj}\left(\frac{b_{ST}}{r^{3}_{Si,Tj}} + \frac{c_{ST}}{r^{6}_{Si,Tj}} + \frac{d_{ST}}{r^{12}_{Si,Tj}}\right), \tag{1}$$

where i and j are HF molecules, q_{Vi} is the charge of site V on molecule i, q_{Wi} is the charge of site W on molecule j, $r_{Vi,Wj}$ is the distance between site V on molecule i and W on molecule j, the atom parameters are b, c, d with the subscripts indicating the type of atom, $r_{Si,Tj}$ is the distance between atom S on molecule i and T on molecule j; these parameters are recorded in Table 1.

As mentioned above, this is a three-site model with charges placed on the fluorine and hydrogen atom centers. The neutralizing charge is placed 0.416 Å from the F atom away from the H atom along the bond axis. The spherical cutoff radius used in the simulations has been specified as 7.6166 Å and, as the potential was developed without any long-range correction for truncation, no such corrections were applied here.

Table 1
Potential parameters for J79

	Parameter		
	FF	FH	HH
b	211.138	−236.016	260.895
c	−641.876	42.221	−356.263
d	255 649.5	2035.165	6363.990
	q_{F}	q_{neutral}	q_{H}
	−61.89676	38.29653	23.60023

The parameters correspond to energy in kJ/mol.

2.2. M.E. Cournoyer and W.L. Jorgensen (CJ84)

The second pair potential studied is a simple, effective model due to Cournoyer and Jorgensen [8]. These authors chose to describe a HF molecule with three charge sites resulting in nine coulombic interactions between two molecules. Additionally, Lennard–Jones (LJ) interactions were added between the fluorine atoms on each molecule. Thus the interactions between two molecules is

$$u_{ij} = \sum_{Vi} \sum_{Wj} \left(q_{Vi} q_{Wj} e^2 / r_{Vi,Wj} \right) + A r_{\mathrm{FF}}^{-12} - C r_{\mathrm{FF}}^{-6} \tag{2}$$

where i and j are two monomers, q_{Vi} is the charge of site V on molecule i, q_{Wj} is the charge of site W on molecule j, $r_{Vi,Wj}$ is the distance between sites V on molecule i and W on molecule j, e is the electrostatic charge, and A and C are LJ parameters.

Unlike the previous work of Jorgensen described above in fitting a HF intermolecular potential, the parameters in this model were determined by performing numerous constant pressure, constant temperature Monte Carlo (MC) simulations and modifying the potential parameters to yield acceptable results for the liquid relative to experimental data. In all simulations, the bond length was held constant at 0.917 Å. A charge of $+0.725e$ is placed on both the fluorine and hydrogen atom centers. The neutralizing charge is placed 0.166 Å from the F atom toward the H atom along the bond axis. The fitted parameters have values of $A = 1.255 \times 10^6$ kJ Å^{12}/mol and $C = 1778$ kJ Å^6/mol. A spherical cutoff radius of 8.0 Å was used for all the simulations of this potential.

Following the development of the potential, a long-range correction for only the LJ part was included for interactions beyond the cutoff.

2.3. A.E. Barton and B.J. Howard (BH82)

In 1982, Barton and Howard [12] took the surface of Alexander and DePristo [18] which was derived from *ab initio* work of Yarkony et al. [19] but fit this with molecular beam spectroscopic data for the dimer. This semi-empirical pair potential is given explicitly in terms of four variables: the distance between the center of mass of the two molecules; the two angles between the line connecting the centers of mass and each bond axis; and the dihedral angle. The HF bond length for both molecules is held fixed at 0.9118 Å. Exponential terms are used to capture the repulsion in the potential while the classical electrostatic interaction is given in terms of spherical harmonics. No accounting for dispersive and induction forces are made in this model. We chose a cutoff radius of 9.5 Å and included long-range corrections in terms of orientationally averaged dipole–dipole, dipole–quadrupole and quadrupole–quadrupole energies [20]. The reader is referred to the original article for the complete potential.

3. Simulation details

MC simulations [21] were performed with VLE determined via the Gibbs–Duhem integration (GDI) technique [22] from high to low temperatures. As is custom, the first state point needed to

Table 2
Simulation parameters for the GE and GDI runs for each potential model

Model	GE			GDI						
	N	Equilibration configurations	Production configurations	N_{liq}	N_{vap}	Predictor iteration	Configurations/ predictor iteration	Corrector iterations	Configurations/ corrector iteration	Production configurations
J79	250	5 M	25 M	230	20	1	1 M	10	1 M	1.5 M
CJ84	250	5 M	25 M	225	25	1	1 M	10	1 M	1.5 M
BH82	250	5 M	25 M	218	32	1	500 K	6	500 K	500 K

Under the 'GE' heading is listed the number of particles used in the system, the number of equilibration and the number of production configurations. Under the 'GDI' heading is listed the number of particles in each phase, the number of predictor iterations, the number of configurations used per predictor iteration, the number of corrector iterations, the number of configurations used per corrector iteration, and the number of production configurations used in determining the values reported in this study.

initiate the integration was obtained from a long Gibbs–Ensemble (GE) simulation [23]. Note that we chose the GDI technique over the more common GE technique in order to avoid the particle exchange problems which occur as the density of the liquid phase increases upon decrease in temperature.

Spherical cutoff was used in cubic boxes with the cutoffs determined by the fluorine–fluorine atom distance. During the GE simulations, the ratio of volume moves, displacement moves, rotation moves, and particle exchange moves was $2{:}N{:}N{:}8N$, where N is the number of particles in the corresponding phase. Further simulation details are given in Table 2.

In order to begin the GDI technique, we need to use the equilibrium pressure as calculated from the GE run for each potential. For the J79 and CJ84 models, we used the vapor virial as the saturation

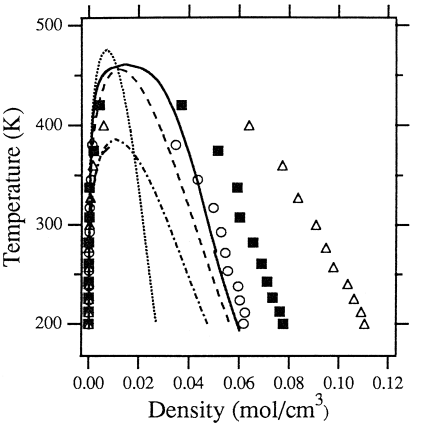

Fig. 1. Coexistence densities as calculated from the various models compared to experimental data. Symbols are from simulation and as follows: open triangles (J79), filled squares (BH82), open circles (CJ84). The lines are as follows: SAFT-HS (P_{sat} optimized) dotted line; SAFT-HS (CJ84 optimized) dash–dot line; SAFT-HS (CJ84 + T_c optimized) dashed line. The experimental results [31–33] are shown as a solid line. Confidence limits of the simulation data are shown only where they are larger than the plotting symbol.

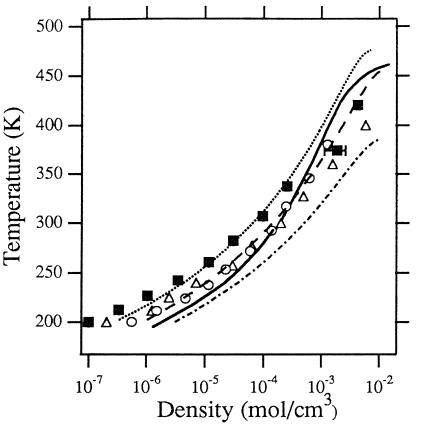

Fig. 2. Saturated vapor densities as calculated from the various models compared to experimental data [31,34]. Symbols and lines are as in Fig. 1.

pressure. Due its complexity, for the BH82 model we instead calculate the pressure via a technique similar [24] to that described by Harismiadis et al. [25].

4. Simulation results

4.1. Coexistence densities

In Fig. 1 we present the saturated densities of the liquid and vapor phases as a function of temperature, calculated from the three potential models and compared to experiment. The effective pair potential (CJ84), which incorporates condensed-phase experimental data implicitly, does a better

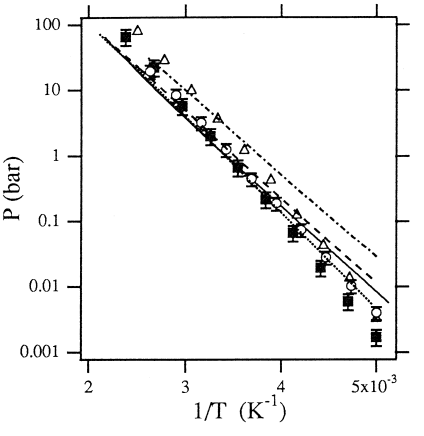

Fig. 3. Vapor pressure as calculated from the various models compared to experimental data [34]. Symbols and lines are as in Fig. 1.

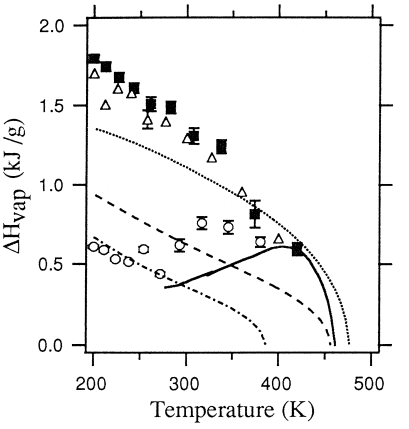

Fig. 4. Vapor pressure as calculated from the various models compared to experimental data [31,35,36]. Symbols and lines are as in Fig. 1.

job on the condensed phase than do the other potentials. The semi-empirical BH82 potential does, in turn, improve upon the estimates of the 'pure' J79 potential. The saturated-vapor density of HF varies over many orders of magnitude for the range of temperatures selected, so we show this property expanded on Fig. 2. It is seen that the effective potential compares most favorably with the experimental data relative to the other models for the vapor density. It seems that the 3 + body interactions, accounted for only by the effective potential, are important in the saturated vapor as well.

4.2. Vapor pressure

In Fig. 3 we present the vapor pressure as calculated from the three potential models compared to that of experiment. None of the models simulated predicts the correct slope in the vapor pressure. Additionally, all of the models show a concave-down shape in the vapor pressure while experiment indicates that this curve is (atypically) concave up.

4.3. Enthalpy of vaporization

The poor prediction of the slope in the vapor pressure by all the models is related, through the Clapeyron equation, to their poor prediction of heat of vaporization, seen in Fig. 4. The effective potential, CJ84, seems to capture the unusual peak in this quantity, albeit at a temperature lower than experiment has determined. The other models, which include only two-body interactions, are not equipped to handle the large reduction in the latent heat at the lower temperatures. This same behavior is seen in engineering equations of state (EOS) that do not adequately account for association [26–28].

5. Discussion

It is clear, and not surprising, that the effective potential CJ84 does a much better job compared to the *ab initio* based models in characterizing the vapor–liquid coexistence properties of HF. Perhaps it

is surprising that CJ84 performs as well as it does, given that its parameters were established by fitting mainly to liquid-phase data (with some attention paid to the gas-phase dimer). Nevertheless there is room for improvement in modeling all VLE properties, particularly the critical temperature, the heat of vaporization and the vapor pressure.

Engineering models of HF have been developed to describe its vapor–liquid coexistence behavior. Most models are based on a chemical equilibrium picture of hydrogen-bond association, and they generally require a significant degree of assumption and parameterization to produce good results. The association scheme requires specification of the types of oligomers present, the equilibrium constants for their interconversion, and mixing rules for how the different oligomers interact. These association models are vastly superior to models that give no acknowledgment to the hydrogen-bonding nature of HF (such as a plain-vanilla cubic EOS), but we have found them lacking in some respects, particularly as concerns heat effects such as the vaporization enthalpy and the superheated-vapor heat capacity [26–28]. We (like many others) feel that the most desirable route to the formulation of an engineering model is via a molecular picture that is as detailed as possible. Such a formulation is most likely to yield results that are consistently good over the broadest range of properties (volumetric, phase equilibria, and heat effects) and, especially important, when extended to mixture behavior.

The SAFT theory is the best present approach to the development of a molecular-based engineering EOS. SAFT has been applied to the description of HF [29], but the focus of that study was the vapor pressure, thus heat effects and densities were not used in establishing the HF EOS. Also, a simplified formulation of the SAFT theory was applied (SAFT-HS), which is based on a hard-sphere molecular model and a first-order perturbation theory that does not account for the formation of ring-shaped clusters. Despite (or because of) the simplicity of this treatment, it is convenient to use it to demonstrate what we might expect in the formulation of a quantitative engineering model from only a quantitative molecular model.

The SAFT-HS treatment for HF models the HF molecule via a hard-sphere repulsive core of diameter σ with an embedded off-center square-well bonding site that is meant to capture the hydrogen-bonding interaction. The site is placed a distance $r_d = 0.25\sigma$ from the center of the hard-sphere and has a cutoff range r_c and well depth ϵ^{hb}. The bonding volume K can be established from these two parameters. The total Helmholtz energy is given as the sum

$$A = A^{ideal} + A^{hs} + A^{assoc} + A^{mf} \tag{3}$$

where ideal, hs, assoc and mf indicate, respectively, ideal-gas, hard-sphere, association, and mean-field contributions. For details we refer the reader to the paper of Galindo et al. [29].

A contour plot of the CJ84 potential is presented in Fig. 5. From this picture we can establish reasonable values for the molecular model used as in input to the SAFT-HS treatment of HF. These values are presented in Table 3, along with the corresponding values proposed by Galindo et al. [29]. The hard-sphere diameter is clear from the contours and differs substantially from the previously proposed value (see Table 3). Our bonding volume K was determined from the volume within the -3 kcal/mol (-12.55 kJ/mol) contour of the CJ84 potential. This cutoff was chosen by examining a histogram of hydrogen-bonding energies observed in our simulations of the CJ84 model [24]. The new volume is roughly four times larger than the previous value. A weighted average of the energies inside the bonding volume sets the value of $\epsilon^{hb} = 16.82$ kJ/mol, roughly equivalent to the SAFT-HS

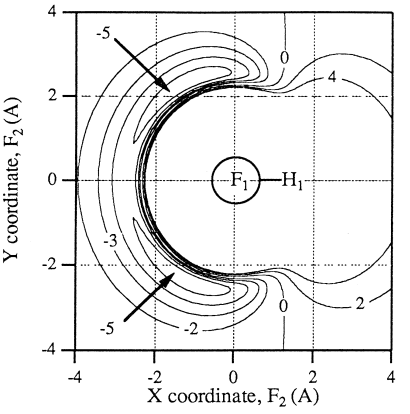

Fig. 5. An energy contour plot of two planar HF molecules from the CJ84 potential model. The energies were determined by rotating a fluorine atom (F_2) around the origin with the hydrogen atom (H_2) pointing towards the origin. Since specific contours were used in the reparameterization of the SAFT-HS parameters, they are left in units of kcal/mol (1 kcal = 4.184 kJ).

value. Finally, the mean-field energy was selected by considering a mean-field description of the fluorine–fluorine LJ r^{-6} interaction, which prescribes $\epsilon = 16\epsilon_{LJ}$, where $\epsilon_{LJ} = 0.6297$ kJ/mol is the LJ energy parameter.

The results from the reparameterized SAFT treatment, named 'CJ84 optimized', are displayed in the figures, along with corresponding results using the original parameters, denoted 'P_{sat} optimized'. Overall, there is improvement, but the performance is still disappointing. The SAFT treatment should in principle describe the CJ84 results. It does get reasonably close to the critical point, but the saturated liquid densities are much too small. Certainly, complete agreement cannot be expected because of the mean-field nature of the analytic SAFT EOS. A contributing factor also is the coarse-graining of the CJ84 potential; the molecular model input to SAFT is only a caricature of the original. We improve the outcome somewhat by adjusting the parameters ϵ and σ to better match the experimental critical temperature, named 'CJ84 + T_c optimized', thereby improving the liquid density, but the comparison to experiment is still not satisfactory. The situation with the vapor densities is

Table 3
The SAFT-HS parameters for HF

	σ (Å)	ϵ/R (K)	ϵ^{hb}/R (K)	K (Å^3)	r_c (Å)	r_d/σ
P_{sat}	3.692	2451	2125	6.6580	2.905	0.25
CJ84	2.984	1212	2023	29.74	3.129	0.25
CJ84 + T_c	2.700	1600	2023	29.74	2.972	0.25

The first row, labelled P_{sat}, are the original parameters from Galindo et al. [29] which were fit to the vapor pressure. The second row, labelled CJ84, are the parameters extracted from the CJ84 potential model [8]. The third row, labelled CJ84 + T_c, uses CJ84 parameters with some parameters modified such that the EOS matches the experimental critical temperature.

not as bad, while the vapor pressure, heat of vaporization and superheated-vapor heat capacity (not shown), all are described unsatisfactorily with the treatment. However, in all cases the results obtained presently, with the SAFT parameters determined from the molecular model, are significantly superior to those obtained with the original parameterization (again keeping in mind that those parameters were determined solely from the vapor pressure, which was the central quantity of interest in the study of Galindo et al. [29]).

6. Concluding remarks

We have determined the coexistence densities, vapor pressure and heat of vaporization from three types of potential models, namely, a pure pair potential, a semi-empirical pair potential, and an effective pair potential. It was found that the effective pair potential was the best performer relative to the two-body potentials, exposing the importance of the 3 + body interactions for HF in both states along the saturation curve.

Further work on two of the potential models presented here, BH82 and CJ84, has been performed to study the importance of clustering, both straight chains and rings, predicted by these models in the superheated vapor phase [24]. It is hoped that agreement amongst several potential models will aid in specifying an association scheme used for HF EOS.

Input from detailed molecular models can be used to establish parameters of molecular-based engineering models, but input from experiment is still needed to produce an EOS with useful descriptive ability. This need can be minimized with the implementation of molecular-based models that are more sophisticated than the SAFT-HS examined here. Variable-range SAFT (SAFT-VR) [30], and treatments that incorporate the higher-order corrections needed to describe oligomer ring formation should be examined as a next step.

7. List of symbols

r	Distance
q	Charge on a site
b, c, d	Atom interaction parameters in J79 potential
A, C	LJ parameters in CJ84 potential
e	Electrostatic charge
σ	Hard-sphere diameter
r_d	Distance from center of sphere to bonding site
r_c	Cutoff range of bonding site
K	Bonding volume
ϵ	Mean field energy parameter
ϵ^{hb}	Well depth
ϵ^{LJ}	LJ energy parameter
A	Free energy
R	Gas constant

Acknowledgements

We acknowledge the Donors of the Petroleum Research Fund, administered by the American Chemical Society, for partial support of this research. Additional support was provided by the National Science Foundation.

References

[1] K. Gubbins, Fluid Phase Equilibria 83 (1993) 1–14.
[2] W.G. Chapman et al., Fluid Phase Equilibria 52 (1989) 31–38.
[3] M.L. Klein et al., J. Chem. Phys. 69 (1978) 63–66.
[4] K. Honda et al., Bull. Chem. Soc. Jpn. 65 (1992) 3122–3134.
[5] W.L. Jorgensen, J. Chem. Phys. 70 (1979) 5888–5897.
[6] U. Rothlisberger, M. Parrinello, J. Chem. Phys. 106 (1997) 4658–4664.
[7] M.L. Klein, I.R. McDonald, J. Chem. Phys. 71 (1979) 298–308.
[8] M.E. Cournoyer, W.L. Jorgensen, Mol. Phys. 51 (1984) 119–132.
[9] S. Murad et al., Chem. Phys. Lett. 131 (1986) 98–102.
[10] P. Jedlovszky, R. Vallauri, J. Chem. Phys. 107 (1997) 10166–10176.
[11] P. Jedlovszky, R. Vallauri, Mol. Phys. 92 (1997) 331–336.
[12] A.E. Barton, B.J. Howard, Faraday Disc. Chem. Soc. 73 (1982) 45–62.
[13] C. Zhang et al., J. Chem. Phys. 91 (1989) 2489–2497.
[14] H. Sun et al., J. Chem. Phys. 96 (1992) 1810–1821.
[15] M. Quack, M.A. Suhm, J. Chem. Phys. 95 (1991) 28–59.
[16] M. Quack et al., J. Mol. Struct. 294 (1993) 33–36.
[17] W. Jorgensen, J. Am. Chem. Soc. 100 (1978) 7824.
[18] M. Alexander, A. DePristo, J. Chem. Phys. 65 (1976) 5009–5016.
[19] D. Yarkony et al., J. Chem. Phys. 60 (1974) 855–865.
[20] G. Maitland et al., Intermolecular Forces, Clarendon Press, New York, 1987.
[21] M.P. Allen, D.J. Tildesley, Computer Simulation of Liquids, Oxford, New York, 1994.
[22] D.A. Kofke, J. Chem. Phys. 98 (1993) 4149–4162.
[23] A.Z. Panagiotopoulos, Mol. Phys. 61 (1987) 813.
[24] D. Visco Jr., D. Kofke, J. Chem. Phys. 109 (1998) 4015–4027.
[25] V.I. Harismiadis et al., J. Chem. Phys. 105 (1996) 8469.
[26] D.P. Visco Jr. et al., AIChE J. 43 (1997) 2381–2384.
[27] D. Visco, Jr., D. Kofke, unpublished results, 1997.
[28] D.P. Visco Jr. et al., Int. J. Thermophys. 19 (1998) 1111–1120.
[29] A. Galindo et al., J. Phys. Chem. B 101 (1997) 2082–2091.
[30] A. Gil-Villegas et al., J. Chem. Phys. 106 (1997) 4168–4186.
[31] E.U. Franck, W. Spalthoff, Z. Electrochem. 61 (1957) 348–357.
[32] I. Sheft et al., J. Inorg. Nucl. Chem. 35 (1973) 3677–3680.
[33] J.H. Simons, J.W. Bouknight, J. Am. Chem. Soc. 54 (1932) 129–135.
[34] C.P.C. Kao et al., Fluid Phase Equilibria 108 (1995) 27–46.
[35] C.E. Vanderzee, W.W. Rodenberg, J. Chem. Thermodyn. 2 (1970) 461–478.
[36] K. Fredenhagen, Z. Anorg. Allg. Chem. 218 (1934) 161–169.